Research Square

Preprints are preliminary reports that have not undergone peer review.
They should not be considered conclusive, used to inform clinical practice,
or referenced by the media as validated information.

Divergent anaerobic fate of biodegradable plastics in landfill leachate

Jaewook Myung

jjaimyung@kaist.ac.kr

KAIST https://orcid.org/0000-0003-2937-1940

Shinhyeong Choe

KAIST https://orcid.org/0000-0002-7279-1644

Hyungmin Choi

Ulsan National Institute of Science and Technology (UNIST)

Hosung Moon

KAIST

Woohyuk Shin

Ulsan National Institute of Science and Technology (UNIST)

Sunho Park

KAIST

Huiju Park

Ulsan National Institute of Science and Technology (UNIST)

Ju Yong Lee

KAIST https://orcid.org/0000-0001-7243-9483

Sukhwan Yoon

Korea Advanced Institute of Science and Technology https://orcid.org/0000-0002-9933-7054

Konstantinos T. Konstantinidis

School of Civil and Environmental Engineering, Georgia Institute of Technology

Changsoo Lee

Ulsan National Institute of Science and Technology (UNIST)

Article

Keywords:

Posted Date: May 4th, 2026

DOI: https://doi.org/10.21203/rs.3.rs-9477234/v1

License: This work is licensed under a Creative Commons Attribution 4.0 International License.
Read Full License

Additional Declarations: There is **NO** Competing Interest.

Version of Record: A version of this preprint was published at Nature Communications on October 20th, 2026. See the published version at https://doi.org/10.1038/s41467-026-78850-w.

Abstract

Biodegradable plastics (BPs) are increasingly promoted as sustainable alternatives to conventional polymers, yet their fate in landfills remains poorly understood. Here, we evaluated the anaerobic biodegradability of three BPs, polyhydroxybutyrate (PHB), poly(lactic acid) (PLA), and poly(butylene adipate terephthalate) (PBAT), in landfill leachate under mesophilic conditions by quantifying carbon conversion to biogas. The BPs exhibited sharply contrasting degradation trajectories: PHB mineralized completely within 17 d, whereas PLA underwent substantial mineralization over 320 d (83.6%), extending beyond the well-established expectation of limited mesophilic degradation. In contrast, PBAT remained largely recalcitrant. Multi-omics analyses linked PHB and PLA depolymerization to the biofilm–polymer interface and to a narrower transcriptionally active subset of the leachate microbiome. Putative depolymerase homologs were widespread across recovered bacterial genomes, but transcriptional support was restricted to a smaller set of genomes, predominantly within Bacillota and Pseudomonadota. This active fraction also included multiple under-characterized lineages with limited representation in current reference databases, revealing a marked disconnect between genomic potential and realized activity. Our findings show that anaerobic biodegradation outcomes in landfill leachate cannot be inferred from biodegradability labels or genomic potential alone, but depend on polymer-specific depolymerization constraints and a narrow biofilm-associated active fraction.

Introduction

Plastic pollution is ubiquitous and poses a planetary-scale threat to ecosystems because conventional plastics, such as low-density polyethylene (LDPE), persist and accumulate across environments [1, 2, 3]. Biodegradable plastics (BPs) have emerged as sustainable alternatives, designed to undergo microbial conversion into benign end products through sequential steps: biodeterioration, depolymerization, bioassimilation, and mineralization [4, 5]. Biodegradation of BPs is determined not only by physicochemical constraints (e.g., chemical structure, molecular weight, and crystallinity) but also by microbial community composition and function. The markedly different degradation rates of chemically identical BPs across environments underscore the limitations of polymer-centered assessments and highlight the need to identify the microbial taxa and functions that mediate BP biodegradation [6, 7].

Among BPs, polyhydroxybutyrate (PHB), polylactic acid (PLA), and poly(butylene adipate-co-terephthalate) (PBAT) have drawn particular attention for their environmental degradability, practical applicability, and industrial scalability [6, 8]. PHB, a microbially synthesized polyester, undergoes rapid degradation in both engineered waste-treatment systems and natural environments [7], making it a benchmark material for biodegradability. In contrast, PLA and PBAT show limited biodegradation in soil and aquatic environments. PLA biodegradation is typically constrained under mesophilic conditions because hydrolytic depolymerization is limited below its glass transition temperature (~58 °C), with efficient degradation reported primarily under thermophilic conditions [9, 10, 11]. PBAT likewise

exhibits effective degradation only under industrial composting conditions [6, 12]. These contrasts suggest that commercial BPs may not share a common fate under anaerobic landfill conditions.

Approximately 103 million tonnes (Mt) of plastic waste were deposited across an estimated 300,000–500,000 landfill sites globally in 2022 [13, 14]. With insufficient waste separate collection and limited access to industrial composting, BPs are often co-disposed with municipal solid waste and routed to landfills. Although landfills represent a major end-of-life destination for BPs, their biodegradation dynamics remain poorly understood, including the key microbial taxa involved in biodegradation. Therefore, elucidating the biodegradation of BPs under landfill conditions is essential for predicting persistence and biogas production potential, thereby supporting environmental impact assessment and waste management strategies.

In contrast to well-characterized engineered waste-treatment systems, such as wastewater treatment and anaerobic digestion [9, 11, 15], genome-resolved microbial ecology studies linking biodegradation processes to landfill microbiomes remain comparatively limited. Landfills are highly heterogeneous and exhibit strong physicochemical gradients [16, 17]. Layered deposition of diverse wastes further increases spatial and temporal variability in nutrient availability, moisture, and redox conditions, complicating representative sampling, reproducible laboratory simulation, and mechanistic inference [17, 18].

Landfill leachate is a nutrient- and contaminant-rich byproduct that captures key chemical and microbial features of landfill environments, and serves as a tractable inoculum for studying landfill-associated microbiomes under laboratory conditions [19, 20]. Chronic exposure to environmental stressors, such as salinity, variable pH, heavy metals, humic substances, and synthetic polymers, shapes the leachate microbial community into a phylogenetically and functionally specialized consortium capable of degrading recalcitrant organic compounds [16, 21, 22]. Recent metagenomic surveys indicated that landfill leachate microbiomes harbor phylogenetically diverse lineages, many of them previously uncultured, with genomic potential for plastic degradation [16, 22, 23]. Collectively, these findings identify landfill leachate as a relevant reservoir of uncharacterized biodegradation functions and as an experimentally tractable inoculum for landfill-derived consortia.

Given that landfills are a major end-of-life destination for biodegradable plastics, yet the microbial basis of their anaerobic degradation remains unresolved, we hypothesized that commercial BPs would follow distinct anaerobic degradation trajectories in landfill leachate. In this study, we incubated PHB, PLA, and PBAT under mesophilic anaerobic conditions and tracked polymer transformation and mineralization over time. To resolve why these polymers diverged in anaerobic biodegradation outcomes, we integrated 16S rRNA gene and rRNA profiling, genome-resolved metagenomics, and metatranscriptomics across biofilm-associated and free-living fractions. This framework linked polymer-specific biodegradation outcomes to active microbial populations and candidate depolymerization functions at the biofilm–polymer interface, while distinguishing broad genomic potential from realized depolymerization activity.

Results

Biodegradable plastics showed sharply divergent anaerobic fates in landfill leachate

The tested biodegradable plastics showed sharply divergent anaerobic fates over 320 d in landfill leachate under mesophilic anaerobic conditions (Figs. 1 and S1). PHB and PLA showed pronounced biogas production, whereas PBAT and LDPE remained close to inoculum-only controls throughout the incubation, with negligible mineralization (2.7% and 0.4%, respectively).

PHB exhibited rapid and near-complete mineralization, reaching 99.9 ± 0.3% within 17 d (Fig. 1a and b). During the initial 5 d, soluble organic carbon (SOC) increased together with short-chain fatty acids (SCFAs, from 46.5 mg C/L in the leachate inoculum to 151.8 mg C/L), indicating early accumulation of soluble intermediates from rapid depolymerization, while mineralization remained minimal during this period (Figs. 1c and S2). SCFAs accumulated further to 2.7 ± 0.0 g C/L at 10–15 d, with acetate and butyrate accounting for >96.0% (Table S1), and then declined rapidly between 15 and 21 d in parallel with a sharp increase in biogas production, reflecting the subsequent activation of methanogenesis. SOC followed a similar temporal pattern, increasing during the early stage and subsequently declining as mineralization progressed. These patterns suggest that rapid depolymerization sustained the supply of soluble intermediates, enabling downstream methanogenesis and driving effective PHB mineralization.

PLA degraded more slowly, yet reached 83.6 ± 1.0% mineralization over 320 d, after an approximately 20 d lag phase during which mineralization remained minimal (0.4%) (Figs. 1b and S2). Following this lag phase, biogas production increased progressively over the remainder of the incubation. At 30 d, SOC increased more strongly than SCFAs, whereas SCFAs returned to near-background levels by 60 d and did not accumulate thereafter (Table S1). This indicates that a substantial fraction of depolymerization-derived intermediates accumulated as SOC, with limited conversion to SCFAs during the early phase of PLA degradation. Lactate, a reported intermediate of PLA depolymerization, remained below 1 mg C/L throughout the incubation, indicating its rapid turnover in this system [24]. These patterns indicate that, unlike PHB, early-stage PLA degradation was characterized by accumulation of depolymerization-derived intermediates as SOC, whereas later stages appeared to be limited by slow depolymerization.

Structural deterioration was rapid in PHB but slower and more heterogeneous in PLA

Distinct structural and surface degradation patterns were observed among the tested plastics during anaerobic incubation (Figs. 2a, S3, and S4). PHB exhibited rapid and pronounced deterioration, with localized roughening and pit formation evident by 10 d, followed by extensive erosion, cavities, matrix fragmentation, and near-complete disintegration by 15–21 d. In contrast, PLA remained largely intact during the early incubation period, showing only minor surface roughening at 30 d. With extended incubation, deeper fissures and scattered pits became evident by 60 d, progressing to pronounced lamellar peeling, enlarged surface defects, and cavities by 170 d. Meanwhile, PBAT and LDPE maintained smooth, intact surfaces throughout incubation, with no visible deterioration. These observations show

that structural deterioration progressed rapidly in PHB but more gradually in PLA, whereas PBAT and LDPE showed little detectable change under the same conditions.

PLA surface degradation was consistently reproduced in independent microcosm experiments inoculated with landfill leachate collected on different dates under identical conditions (Figs. 2b and S5). After 90 d of incubation, surface micrographs revealed dense colonization by rod-shaped bacteria and extensive biofilm formation on the PLA surface, with cells closely associated with damaged regions of the polymer matrix. These images provide direct visual evidence that PLA degradation in landfill leachate was concentrated at the biofilm–polymer interface, linking microbial colonization to the progressive surface deterioration and mineralization (Fig. 1).

FT-IR spectra further supported polymer-specific structural alteration during incubation (Figs. 2c and S6). PHB and PLA showed clear time-dependent changes in the carbonyl (C=O) stretching region (1700–1750 cm^{-1}), whereas PBAT and LDPE showed little detectable spectral variation over the same period. In PHB, attenuation of the carbonyl band was already evident by 10 d and became more pronounced by 15 d, consistent with its rapid mineralization and surface disintegration. In PLA, carbonyl-band attenuation progressed more gradually through 60 d. By 170 d, the carbonyl region showed a partial recovery in transmittance, consistent with relative enrichment of more degradation-resistant residual domains as degradation progressed. Together, these spectral patterns support rapid and extensive structural breakdown of PHB but a slower and more heterogeneous transformation of PLA under mesophilic anaerobic conditions.

Biofilm and free-living microbiomes differed in composition and activity during PHB and PLA degradation

The divergent degradation patterns of PHB and PLA were accompanied by marked differences between polymer-associated biofilms and the surrounding free-living microbiomes (Fig. 3 and Tables S2). Across 16S rRNA gene (DNA) and 16S rRNA (RNA converted to cDNA) amplicon sequencing and shotgun metagenomic sequencing profiles, this lifestyle-associated differentiation was consistently evident.

16S rRNA gene profiles showed strong early enrichment of Pseudomonadota in biofilms on both PHB and PLA, followed by increasing contributions from Bacillota, Bacteroidota, and methanogen-associated phyla at later stages. In contrast, free-living communities were more consistently dominated by Bacillota and showed less pronounced early enrichment of Pseudomonadota, indicating that lifestyle-associated differences were strongest during the early stages of degradation.

The compositional contrasts were more pronounced in 16S rRNA profiles, which captured the putatively active fraction (Figs. 3b and S7). PHB biofilms showed strong early activity of Pseudomonadota during 5–10 d, whereas PLA biofilms showed a distinct early enrichment of Desulfobacterota. At later stages, both systems shifted toward Bacillota, Bacteroidota, and methanogen-associated archaeal lineages. These results suggest that similar early surface colonization did not translate into the same active community structure across polymers [25].

Shotgun metagenomic profiles broadly reproduced the dominant community patterns observed in the DNA-based amplicon datasets (Figs. 3c and d). Across assays, both read- and metagenome-assembled genome (MAG)-based profiling recovered Pseudomonadota and Bacillota as major components, consistent with the 16S-derived trends. Shotgun data further highlighted lineages that were less apparent in the amplicon profiles, including methanogen-associated Methanobacteriota in read-based classification and Halobacteriota in MAG-based profiles. Substantial fractions, nevertheless, remained unclassified or unmapped across shotgun approaches (Fig. S8), indicating incomplete reference coverage for this microbiome. These analyses show that the major community patterns were reproducible across sequencing approaches, while shotgun profiling provided additional taxonomic resolution.

Biofilm and RNA-derived communities represented narrower subsets of the landfill leachate microbiome during biodegradation

Based on 16S rRNA (gene) amplicon profiles, microbial diversity differed both between biofilm and free-living communities and between DNA- and RNA-derived communities (Fig. 4 and Table S4). Across substrates, biofilm communities exhibited significantly lower Shannon diversity and Faith's phylogenetic diversity than free-living assemblages (Wilcoxon test, $P < 0.01$), consistent with selective enrichment of a taxonomically and phylogenetically narrower subset of lineages at the polymer surface (Table S5). RNA-derived communities were likewise significantly less diverse than DNA-derived profiles ($P < 0.001$), indicating that transcriptionally active populations represent a metabolically narrower fraction of the overall community.

Community dissimilarity analyses further supported these differences (Fig. 4b and Table S5). Bray–Curtis distances revealed significant substrate effects on taxonomic composition (PERMANOVA, $P < 0.05$), with differences in dispersion across substrates (PERMDISP, $P < 0.01$) (Fig. S9). In contrast, weighted UniFrac highlighted nucleic acid-dependent differences in phylogenetic structure, with significant differences in dispersion between DNA- and RNA-derived communities (PERMDISP, $P < 0.01$) despite non-significant centroid shifts. Together, substrate type primarily shaped overall community composition, whereas DNA- and RNA-derived assemblages diverged more clearly in phylogenetic structure.

Depolymerase transcription was enriched in biofilms and tracked PHB and PLA degradation phases

To connect the community-level contrasts above with functional activity, we next examined transcriptional profiles of enzyme families implicated in anaerobic plastic degradation across biofilm and free-living fractions (Fig. 5a, Tables S6 and S7). Across the curated enzyme families, protease-related transcripts were broadly detected, whereas transcripts assigned to substrate-associated depolymerases showed clearer temporal coupling to PHB and PLA. Depolymerase transcripts were enriched in biofilm communities and aligned with the observed degradation phases of each polymer.

In PHB incubations, biofilm-associated PHB-depolymerase transcripts were highest at 5 d, whereas the free-living fraction showed elevated transcription at 5–10 d followed by a marked decline after 15 d. In PLA incubations, PLA-depolymerase transcripts were most prominent in biofilm transcriptomes from 60 to 170 d, coinciding with the active mineralization phase, whereas free-living fractions showed lower but sustained transcription during 30–170 d. These temporal patterns suggest that depolymerase transcription was concentrated in biofilms, with related transcriptional activity extending into the free-living fraction.

Differential expression analysis further supported lifestyle partitioning of biodegradation-linked enzymes (Fig. 5b and Table S8). In PHB incubations, multiple PHB-depolymerase representatives were significantly upregulated in biofilm relative to free-living samples (DESeq2, FDR-adjusted $P < 0.05$; $\log_2$ fold change > 1). In PLA incubations, fewer representatives exceeded the significance threshold, but several PLA-depolymerase and protease representatives were likewise enriched in biofilm. Because several reported PLA depolymerases belong to serine protease families, these protease signals may partly reflect PLA-associated depolymerization activity, although annotation alone could not resolve substrate specificity. Limited replication in PLA biofilms ($n = 2$) likely reduced power to detect differential expression in PLA incubations (Table S3).

Phylogenomic narrowing from homolog-carrying genomes to transcription-supported lineages

Genome-resolved screening of the dereplicated MAG set ($n = 238$) identified putative PHB- and PLA-depolymerase homologs in 118 recovered lineages spanning multiple phyla, indicating a broad genomic reservoir of candidate depolymerization functions (Fig. S10 and Table S9). PLA-associated homologs were detected in substantially more MAGs ($n = 111$) than PHB-associated homologs ($n = 16$), with 9 MAGs carrying both. However, this difference likely reflects properties of the reference space used for homology detection rather than intrinsic polymer degradability, and should not be interpreted as proportional to true enzyme diversity or biodegradation potential (Figs. S11 and S12).

Transcriptional support defined a much narrower subset of this reservoir. Among the 118 homolog-carrying MAGs, only 49 showed depolymerase transcriptional support (TPM ≥ 1), indicating a marked narrowing from genomic potential to expressed activity (Fig. 6a). Notably, 37 of these 49 MAGs were assigned to GTDB placeholder taxa, indicating substantial contributions from lineages that remain poorly represented in the current genome repository.

This transcription-supported subset was phylogenetically distinct from the experimentally validated degrader genomes curated in public reference databases including PlasticDB and PAZy. The reference set was concentrated in Pseudomonadota and Bacilli and dominated by aerobic or facultatively anaerobic isolates. In contrast, the transcription-supported MAGs recovered here were enriched in Bacillota and extended into anaerobic classes, including Clostridia, Peptococcia, and Limnochordia, with additional representation from Pseudomonadota, Bacteroidota, Chloroflexota, and Spirochaetota (Fig. 6a). Pseudomonadota, despite dominating the early biofilm communities in both PHB and PLA incubations (Fig. 3), showed depolymerase transcription in only two Gammaproteobacterial MAGs,

indicating that broad community dominance did not necessarily correspond to transcriptional engagement in depolymerization. These comparisons indicate that anaerobic BP depolymerization in landfill leachate is confined to a phylogenetically restricted and largely under-characterized subset of the broader homolog-carrying community.

Time-series integration resolved polymer-specific candidate MAGs linked to depolymerization

Integration of MAG-level coverage with depolymerase transcription across the incubation time series resolved a distinct set of polymer-associated candidate MAGs (Fig. 6b and Table S10). These candidate MAGs were selected based on elevated depolymerase transcription and were then evaluated together with sample-resolved MAG coverage across each polymer incubation. This analysis revealed clear temporal partitioning, with PHB-associated candidate MAGs peaking early and PLA-associated candidates emerging later during the sustained mineralization phase.

In PHB incubations, the most prominent candidate MAGs were concentrated within Bacillota lineages spanning Peptococcia and Clostridia, together with an early Gammaproteobacterial contributor. MAG034 showed the highest PHB-depolymerase transcription during the early phase and peaked in abundance at 5–10 d, consistent with a primary role during initial PHB depolymerization. Several Bacillota MAGs, including MAG120, MAG121, and MAG111, remained prominent across PHB incubations, indicating that PHB depolymerization involved both early-colonizing and persistent anaerobic lineages. These PHB-associated candidate MAGs showed little coverage in PLA incubations, supporting polymer specificity.

PLA-associated candidate MAGs were likewise dominated by Bacillota but emerged later and remained prominent through the sustained mineralization phase. MAG126 was nearly absent at day 5 but appeared from day 30 onward, coinciding with sustained mineralization and showing strong PLA-depolymerase transcription where metatranscriptomes were available. MAG063 showed a similar PLA-associated pattern, particularly in the free-living series. In contrast, MAG031 displayed an early-colonizer profile, peaking at day 5 and remaining detectable thereafter, consistent with a role in the initial stage of PLA depolymerization rather than the prolonged active phase. Although metatranscriptomes were unavailable for BD_PLA_5 and BD_PLA_30, the combined coverage and transcription patterns still resolved a coherent PLA-associated candidate set distinct from the PHB-associated group.

Overall, this time-series integration resolved distinct PHB- and PLA-associated candidate MAGs with contrasting temporal signatures, narrowing the broader homolog-carrying community to a smaller transcription-supported subset.

Ecological distribution of genomes encoding PHB- and PLA-depolymerase homologs

Genomes encoding PHB- and PLA-depolymerase homologs were distributed across diverse ecosystem contexts and geographic regions beyond the landfill-derived MAGs recovered in this study (Fig. 7 and Table S11). Using depolymerase-positive MAGs recovered in this study as query lineages, targeted genome mining across public genome collections identified genomes encoding PHB-depolymerase

homologs (*n* = 366) and PLA-depolymerase homologs (*n* = 1,655) across engineered systems, environmental samples, and host-associated microbiomes.

Engineered anaerobic settings, including anaerobic digestion systems, wastewater and sludge environments, and landfill-derived habitats, accounted for a substantial fraction of the compiled records. Environmental records were also common across sediment, groundwater, terrestrial, freshwater, and marine-associated compartments, and host-associated records were additionally recovered from gut-associated, oral, and clinical/body-site microbiomes. The larger number of PLA-associated genomes relative to PHB-associated genomes likely reflects reference-bounded detection sensitivity, shaped by reference-set size and architecture, rather than intrinsically greater PLA degradability (Figs. S11 and S12). Collectively, these records indicate that depolymerase-encoding lineages are broadly distributed across engineered and oxygen-limited environments, with additional representation in host-associated and other environmental microbiomes.

Discussion

PHB, PLA, and PBAT did not exhibit a uniform anaerobic fate in landfill leachate. The degradation trajectories were strongly polymer-specific, with rapid mineralization of PHB (99.9% within 17 d), substantial but delayed mineralization of PLA (83.6% over 320 d), and negligible transformation of PBAT (Fig. 1). This divergence indicates that persistence of BPs is governed by polymer-dependent constraints on depolymerization and subsequent microbial conversion under oxygen-limited conditions. Recent work in anaerobic digestion and other environmentally relevant systems has likewise shown that biodegradable plastics can follow distinct transformation trajectories [11, 29, 30]. Our results extend these observations to a landfill-derived mesophilic anaerobic microbiome and show that polymer-specific differences remain evident even under a single inoculum and incubation regime. In this sense, “biodegradable plastics” do not constitute a functionally coherent end-of-life category in landfill environments [31].

These polymer-specific outcomes have direct implications for environmental performance and waste management. In particular, materials grouped under the same biodegradability label can follow fundamentally different carbon fates under anaerobic landfill conditions: carbon may be mineralized to biogas, transiently accumulate in soluble intermediates, or remain as persistent polymer residue (Fig. 1c and Table S1). Where mineralization occurs, environmental benefit depends on gas capture and management; where degradation is slow or absent, marketed biodegradability may not translate into meaningful mitigation of long-term plastic accumulation after disposal. This mismatch between shared labeling and divergent carbon fates represents a central practical implication of our data and argues for end-of-life evaluation frameworks that explicitly consider anaerobic conditions in landfill systems, particularly because current labeling schemes are centered primarily on composting and do not directly address landfill disposal outcomes [32].

At the microbiological level, this study shows that anaerobic depolymerization is mediated by a highly selective transcriptionally active fraction of the landfill leachate microbiome. Depolymerase-associated genes were broadly distributed across recovered MAGs, yet transcriptional support was restricted to a narrower set of lineages, and depolymerase expression was concentrated at the biofilm–polymer interface (Figs. 3–6) [31]. This marked decoupling between homolog carriage and realized activity indicates that anaerobic plastic depolymerization cannot be inferred from genomic potential alone, but depends on selective activation of populations at the polymer-associated interface [16, 33].

The transcriptionally active subset identified here was also phylogenetically restricted and enriched in under-characterized lineages. The predominance of GTDB placeholder taxa among transcription-supported candidate MAGs indicates that key anaerobic depolymerization functions remain poorly represented in current reference databases [22]. Consistent with this interpretation, lineages carrying PHB- and PLA-depolymerase homologs were broadly distributed across public genome collections, whereas realized activity under the conditions examined here was restricted to a much narrower subset (Fig. 7) [22, 34].

These conclusions should be interpreted within the constraints of the experimental system. Landfill leachate incubations under mesophilic anaerobic conditions do not reproduce the full spatial and physicochemical heterogeneity of landfill environments, including temperature variability, diffusion limitations, microscale redox gradients, heterogeneous solid–liquid interfaces, and waste-matrix complexity, which can influence microbial colonization, syntrophic interactions, and rate-limiting steps. As such, the biodegradation kinetics reported here should not be extrapolated as quantitative predictions of in situ landfill behavior. In addition, depolymerase candidates were assigned by homology, and many fell within moderate similarity ranges relative to curated references (Figs. S11 and S12). These sequences are therefore interpreted as putative depolymerization functions, and the catalog reported here represents a conservative, reference-constrained estimate rather than a comprehensive inventory of anaerobic depolymerization capacity. Nevertheless, the controlled landfill leachate system used here enabled mechanistic resolution that would be difficult to achieve directly in intact landfill matrices, particularly for linking mineralization trajectories to biofilm-associated transcription and genome-resolved candidate lineages (Figs. 5 and 6).

The substantial mineralization of PLA under mesophilic anaerobic conditions extends beyond the well-established expectation of limited PLA mineralization under non-thermophilic conditions (Fig. 1) and identifies microbiome context as a critical determinant of whether physicochemical barriers are overcome [7, 9, 11, 29, 30]. Although PLA degradation was examined here in a single-substrate system, these findings may also have implications for engineered anaerobic processes. Prior work suggests that co-digestion with readily biodegradable food substrates does not necessarily overcome mesophilic limitations on PLA degradation [11]. As such, our results suggest that the distinct microbial composition of landfill leachate, together with biofilm-localized depolymerase expression, may have enabled substantial PLA conversion under mesophilic anaerobic conditions. This interpretation is further

supported by reports of incomplete PLA degradation and microplastic persistence in mesophilic anaerobic digestion, indicating that favorable bulk anaerobic activity alone is insufficient when populations capable of initiating depolymerization are absent. Microbial sources enriched in populations capable of initiating PLA depolymerization may therefore represent promising candidates for future bioaugmentation or enrichment strategies in engineered anaerobic digestion, although this remains to be tested directly. Further work is warranted to determine how inoculum source and enrichment history shape PLA transformation under mesophilic anaerobic conditions.

Taken together, these findings provide a mechanistic basis for interpreting the anaerobic fate of biodegradable plastics in landfill environments. More broadly, our results show that anaerobic fate is not an intrinsic property of a biodegradable plastic alone, but an emergent outcome of polymer chemistry, microbiome context, and selective activation at the biofilm–polymer interface.

Materials and Methods

Plastic film fabrication and characterization

Three BPs (PHB, PLA, PBAT) and LDPE films were fabricated from individual polymer pellets (Table S12). A laboratory-scale twin-screw extruder BA-19 (BauTech Co., Republic of Korea) was employed for homogeneous mixing and dispersion with a length-to-diameter ratio of 40:1. The extrusion temperature profile was optimized for each plastic type (Table S13). The thickness of each film was measured 10 times using a digital thickness gauge PK-1012APX (Mitutoyo Co., Japan). The films were sterilized using 70% ethanol and subsequently air-dried in a biosafety cabinet prior to incubation. The carbon, hydrogen, and nitrogen contents (%) of plastic films were measured using a FLASH 2000 elemental analyzer, and the oxygen content (%) was quantified using a FlashSmart elemental analyzer (Thermo Fisher Scientific, USA).

Sampling and pre-incubation of landfill leachate

Landfill leachate was sampled in June 2024 at the leachate collection sump of the Buyeo sanitary landfill (36.2019° N, 126.9333° E), which has been in operation since 1997 (Fig. S1a). Two 5 L media bottles were each filled with 4 L of leachate and purged with ultra-pure N_2 gas for 10 min to remove residual O_2. To minimize endogenous biogas production from residual labile organics, the leachate was pre-incubated for 17 d, during which the bottles were sealed gas-tight with rubber stoppers connected to gas-sampling bags, incubated at 35 °C, and manually shaken once a day (Fig. S1b). A total of 1,804 ± 55 mL of biogas was produced without nutrient addition (Fig. S1c). The pre-incubated landfill leachate was characterized (Table S14), and immediately used as the inoculum for the anaerobic degradation assays.

Anaerobic biodegradation tests

BP films (PHB, PLA, and PBAT) and LDPE, used as a negative control, were subjected to batch anaerobic biodegradation assays with eight replicates per treatment (Fig. S1e). The tests were performed in 280

mL serum bottles with a 200 mL working volume and 80 mL of headspace, following ISO standard protocol [35]. Each bottle was loaded with 1.2 g of plastic film strips (1 cm × 4.5 cm) and 200 mL of pre-incubated landfill leachate (100% *v*/*v*). The bottles were purged with ultra-pure N_2 gas for 2 min to remove residual O_2, and sealed gas-tight with butyl rubber septa and aluminum crimps. The incubations were conducted at 35 °C, with bottles manually shaken twice a day. Five sets of assays were conducted in parallel, including an inoculum-only blank assay in triplicate (Fig. S1e). Blank assays were used to account for endogenous biogas and methane production from the inoculum. To assess the anaerobic degradation of plastic films, both the plastic and mixed liquor (i.e., leachate) were sacrificially sampled on 5, 10, and 15 d for PHB assay, and on 5, 30, 60, 100, and 170 d for PLA, PBAT, and LDPE assays. The retrieved plastic samples at each sampling point were gently washed three times with phosphate-buffered saline (100 mM, pH 7.4) and immediately subjected to further analyses.

Biogas production from each bottle was monitored using a manometric measurement method, with a gas-tight three-way valve connected to a syringe needle and a pressure gauge (Fluke, USA, 700G05). Produced biogas was periodically collected with a gas-tight syringe, and biogas composition (H_2, CH_4, CO_2, and H_2S) was analyzed using a 490 MicroGC system (Agilent, USA) equipped with thermal conductivity detectors connected to two columns, a CP-Molsieve 5Å and a CP-PoraPLOT U (Agilent, USA), respectively. All biogas and methane volumes were reported after correction to standard temperature and pressure (0 °C and 1 bar).

Biodegradation level was calculated as the ratio of the observed biogas production to the theoretical maximum biogas production. The theoretical values were estimated based on the elemental composition of the plastics using the extended Buswell and Mueller equation [35] (Eq. 1):

$$C_cH_hO_oN_nS_s + \left(c - \frac{h}{4} - \frac{o}{2} + \frac{3n}{4} + \frac{s}{2}\right)H_2O \rightarrow \left(\frac{c}{2} + \frac{h}{8} - \frac{o}{4} - \frac{3n}{8} - \frac{s}{4}\right)CH_4 + \left(\frac{c}{2} - \frac{h}{8} + \frac{o}{4} + \frac{3n}{8} + \frac{s}{4}\right)CO_2 + nNH_3 + sH_2S \quad \text{(Eq. 1)}$$

where *c*, *h*, *o*, *n*, and *s* represent the atomic counts of carbon, hydrogen, oxygen, nitrogen, and sulfur, respectively. The values of *c*, *h*, and *o* were normalized to sum to 100%, while *n* and *s* were set to zero based on the empirical formulas of the plastics (Table S13).

Physicochemical analyses of landfill leachate

Landfill leachate pH was measured using an Orion 3-Star pH meter (Thermo Scientific, USA), and alkalinity was determined with the Orion Total Alkalinity Test Kit (Thermo Scientific, USA). Solids were analyzed according to the Standard Methods for the Examination of Water and Wastewater [36]. Chemical oxygen demand, nitrogen, and phosphorus were measured using HS-COD-MR, HS-TN(CA)-H, and HS-TP-H kits, respectively (Humas, South Korea). Volatile fatty acids (C_{2-7}) were quantified using a 7820A gas chromatograph (Agilent, USA). Lactate was analyzed using the D-/L-Lactic Acid (D-/L-Lactate) (Rapid) Assay Kit (Megazyme, K-DLATE). Samples for soluble chemical oxygen demand, nitrogen, phosphorus,

volatile fatty acids, and lactate analyses were pre-filtered through 0.45-μm membrane filters. SOC content was measured using a TOC-V CPH analyzer (Shimadzu, Japan). Ionic species were analyzed using dual Dionex ICS-1100 ion chromatographs equipped with IonPac AS14 (for anions) and CS12A (for cations) columns (Thermo Scientific, USA), respectively. Samples for SOC and ion analyses were pre-filtered through 0.22-μm membrane filters. Heavy metal concentrations were determined using an inductively coupled plasma optical emission spectrometry (Varian, 700-ES, USA).

Morphological and structural characterization

The plastic films for surface morphology monitoring, retrieved during the biodegradation test, were transferred into a freshly prepared 2.5% paraformaldehyde-glutaraldehyde fixing solution, washed with 0.1 M phosphate buffer (pH 7.2) for 10 min. The films were postfixed in the same buffer containing 1% osmium tetroxide at 25 °C for 1 h. The samples were then dehydrated with a series of increasing concentrations of ethanol/isoamyl acetate solutions (30, 50, 70, 80, 98, and 100% for 10 min, respectively), followed by critical point drying in liquid CO_2 using EM CPD300 (Leica, Germany). Finally, the samples were sputtered with gold in a sputter coater SC502 (POLARON, Canada) and observed using the scanning electron microscope FEI Quanta 250 FEG (FEI, USA) at a magnification of 2,500–10,000×. Characteristic chemical bonds of plastic films were analyzed using Fourier-transform infrared spectroscopy (FT-IR) with a Nicolet iS50 (Thermo Fisher Scientific, USA) in the attenuated total reflection mode over the wavenumber range of 400 to 4,000 cm^{-1}.

Extraction of nucleic acids and sample preparation

Total DNA and RNA were extracted from both the biofilm (plastic-attached biomass) and free-living fractions (mixed liquor) using the RNeasy PowerSoil Total RNA Kit and DNA Elution Kit (QIAGEN, Germany), following the manufacturer's instructions (see Supplementary Notes for details). Sample codes for sequencing analyses were assigned based on four criteria: microbial lifestyle (biofilm or free-living), nucleic acid type (DNA or RNA), plastic substrate type (PHB, PLA, PBAT, LDPE, or blank leachate), and incubation day (Table S3).

16S rRNA (gene) amplicon sequencing

Total RNA was reverse-transcribed into complementary DNA (cDNA) using the SuperPrep II RT Kit for qPCR (Toyobo, Japan). The prokaryotic 16S rRNA genes from both total DNA and cDNA were amplified with the 515F and 806R primer set targeting the V4 hypervariable region [37] (Table S15). The prepared library was then sent to Macrogen Inc. (South Korea), and paired-end sequencing (2 × 300 bp) was performed on the MiSeq platform (Illumina, USA). The amplicon sequence data (n = 76) were analyzed using the QIIME2 pipeline and a custom R script (see Supplementary Notes for details).

Metagenomic and metatranscriptomic sequencing

Metagenomic libraries (*n* = 19) were constructed using the TruSeq Nano DNA (350) kit (Illumina, USA), according to the manufacturer's protocol. Ribosomal RNA was depleted, and reverse-transcribed cDNA libraries (*n* = 15) were prepared using the Illumina Stranded Total RNA Library Prep with Ribo-Zero Plus Microbiome kit (Illumina, USA). Paired-end shotgun sequencing (2 × 150 bp) for both metagenomic and metatranscriptomic libraries was performed on the NovaSeq X platform (Illumina, USA) by Macrogen Inc. (South Korea), with a targeted throughput of 10 Gbp per sample.

Gene-centric depolymerase annotation and transcript quantification

A gene-centric workflow was used to compare depolymerase-associated genomic potential and transcription across samples. Quality-filtered metagenomic reads were assembled, open reading frames (ORFs) were predicted from assembled contigs, and highly similar ORFs were clustered into a non-redundant representative catalog that served as a unified reference for annotation and transcript quantification. A curated reference database of PHB- and PLA-depolymerases was constructed from PlasticDB and PAZy, and representative ORFs were annotated using DIAMOND blastp (≥ 30% amino acid identity, ≥ 50% query coverage, ≤ $1e^{-5}$ e-value). Quality-filtered non-rRNA metatranscriptomic reads were quantified against the same representative nucleotide catalog, and non-rRNA read retention and transcript mapping rates were evaluated across libraries (Fig. S13). Transcript abundance was summarized at both the representative and enzyme-family levels (see Supplementary Notes for details).

Genome-resolved MAG reconstruction and depolymerase profiling

Metagenome-assembled genomes (MAGs) were reconstructed using a consensus binning workflow, dereplicated at 95% average nucleotide identity, and taxonomically classified with GTDB-Tk. MAG abundance and coverage across samples were estimated by read mapping. Coding sequences predicted from each MAG were annotated against the curated PlasticDB–PAZy reference database using the same criteria applied in the gene-centric analysis, and metatranscriptomic reads were quantified against MAG-derived coding sequences to summarize depolymerase-associated expression at the genome level. MAGs were designated as transcriptionally supported when genome-wide depolymerase-associated TPM was ≥ 1. Depolymerase-positive MAGs were further compared with reference genomes encoding experimentally validated depolymerases and used as anchors for targeted genome mining and ecological contextualization (see Supplementary Notes for details).

Declarations

Data availability

All data supporting the findings of this study are available in the Supplementary Information and Supplementary Tables. Raw sequencing data have been deposited in the NCBI Sequence Read Archive (SRA) under BioProject accession numbers PRJNA1395782 (16S rRNA (gene) amplicon sequencing) and PRJNA1403162 (metagenomic and metatranscriptomic sequencing). Any additional data are available from the corresponding authors upon reasonable request.

Code availability

Custom R and Python scripts used for microbial community composition and diversity, depolymerase annotation, transcript quantification, MAG-level profiling, and statistical analyses are available from the corresponding authors upon reasonable request.

Acknowledgements

This work was supported by the Hyundai Motor Chung Mong-Koo Foundation, National Research Foundation of Korea (NRF) grant funded by the Korea government (MSIT) (RS-2023-00209472, RS-2024-00437656, RS-2026-25393325, and RS-2024-00353585), and by the grant for the “KAIST Grand Challenge 30 Program” funded by the Korea Advanced Institute of Science and Technology (N11250072).

Author contributions

S.C. and H.C. conceptualized the study. S.C., H.C., H.M., W.S., and H.P. performed sample preparation, anaerobic biodegradation assay, chemical and morphological analyses. S.C. conducted bioinformatic analyses. S.C. and H.C. wrote the first draft of the manuscript, with input from S.P., J.L., K.K., C.L., and J.M. C.L. and J.M. supervised the project. All authors discussed the results and commented on the manuscript.

Competing interests

The authors declare no competing interests.

References

1. Kaandorp, M.L., Lobelle, D., Kehl, C., Dijkstra, H.A. & van Sebille, E. Global mass of buoyant marine plastics dominated by large long-lived debris. *Nat. Geosci.* **16**, 689–694 (2023).
2. Sheng, D., et al. Plastic pollution in agricultural landscapes: an overlooked threat to pollination, biocontrol and food security. *Nat. Commun.* **15**, 8413 (2024).
3. MacLeod, M., Arp, H.P.H., Tekman, M.B. & Jahnke, A. The global threat from plastic pollution. *Science* **373**, 61–65 (2021).
4. Haider, T.P., Völker, C., Kramm, J., Landfester, K. & Wurm, F.R. Plastics of the future? the impact of biodegradable polymers on the environment and on society. *Angew. Chem. Int. Ed.* **58**, 50–62 (2019).
5. Zumstein, M.T., et al. Biodegradation of synthetic polymers in soils: tracking carbon into CO_2 and microbial biomass. *Sci. Adv.* **4**, eaas9024 (2018).
6. Kim, M.S., et al. A review of biodegradable plastics: chemistry, applications, properties, and future research needs. *Chem. Rev.* **123**, 9915–9939 (2023).
7. Choe, S., Kim, Y., Won, Y. & Myung, J. Bridging three gaps in biodegradable plastics: misconceptions and truths about biodegradation. *Front. Chem.* **9**, 671750 (2021).

8. European Bioplastics. *Bioplastics Market Development Update 2025* (European Bioplastics e.V., Berlin, 2025).
9. García-Depraect, O., et al. Biodegradation of bioplastics under aerobic and anaerobic aqueous conditions: kinetics, carbon fate and particle size effect. *Bioresour. Technol.* **344**, 126265 (2022).
10. Narancic, T., et al. Biodegradable plastic blends create new possibilities for end-of-life management of plastics but they are not a panacea for plastic pollution. *Environ. Sci. Technol.* **52**, 10441–10452 (2018).
11. Zhang, Y., et al. Anaerobic degradation of aromatic and aliphatic biodegradable plastics: potential mechanisms and pathways. *Environ. Sci. Technol.* **58**, 19462–19474 (2024).
12. Kim Y, et al. Biodegradation of poly (butylene adipate terephthalate) and poly (vinyl alcohol) within aquatic pathway. *Sci. Total Environ.* **953**, 176129 (2024).
13. Wang Y, et al. Methane emissions from landfills differentially underestimated worldwide. *Nat. Sustain.* **7**, 496–507 (2024).
14. Houssini, K., Li, J. & Tan, Q. Complexities of the global plastics supply chain revealed in a trade-linked material flow analysis. *Commun. Earth Environ.* **6**, 257 (2025).
15. Wang, S., et al. Biodegradation of poly (3-hydroxybutyrate-co-3-hydroxyhexanoate) plastic under anaerobic sludge and aerobic seawater conditions: gas evolution and microbial diversity. *Environ. Sci. Technol.* **52**, 5700–5709 (2018).
16. Meyer-Dombard, D.A.R., Bogner, J.E. & Malas, J. A review of landfill microbiology and ecology: a call for modernization with 'next generation' technology. *Front. Microbiol.* **11**, 1127 (2020).
17. Sauk, A.H. & Hug, L.A. Substrate-restricted methanogenesis and limited volatile organic compound degradation in highly diverse and heterogeneous municipal landfill microbial communities. *ISME Commun.* **2**, 58 (2022).
18. Grégoire, D.S., George, N.A. & Hug, L.A. Microbial methane cycling in a landfill on a decadal time scale. *Nat. Commun.* **14**, 7402 (2023).
19. Qian, Y., et al. Global landfill leachate characteristics: occurrences and abundances of environmental contaminants and the microbiome. *J. Hazard. Mater.* **461**, 132446 (2024).
20. Deng, C., et al. Genome-centric metagenomics provides new insights into the microbial community and metabolic potential of landfill leachate microbiota. *Sci. Total Environ.* **816**, 151635 (2022).
21. Shen, R., et al. Nationwide screening of landfill-derived organohalide-respiring bacteria elucidates a unique cross-feeding interaction for microbial reductive dehalogenation. *Water Res.* **284**, 123964 (2025).
22. Lin, X., et al. Natural-selected plastics biodegradation species and enzymes in landfills. *PNAS Nexus* **4**, pgaf066 (2025).
23. Stamps, B.W., et al. Municipal solid waste landfills harbor distinct microbiomes. *Front. Microbiol.* **7**, 534 (2016).

24. Shalem, A., Yehezkeli, O. & Fishman, A. Enzymatic degradation of polylactic acid (PLA). *Appl. Microbiol. Biotechnol.* **108**, 413 (2024).
25. Schaerer, L., et al. Coexistence of specialist and generalist species within mixed plastic derivative-utilizing microbial communities. *Microbiome* **11**, 224 (2023).
26. McDonald, D., et al. Greengenes2 unifies microbial data in a single reference tree. *Nat. Biotechnol.* **42**, 715–718 (2024).
27. Wood, D.E., Lu, J. & Langmead, B. Improved metagenomic analysis with Kraken 2. *Genome Biol.* **20**, 257 (2019).
28. Chaumeil, P.A., Mussig, A.J., Hugenholtz, P. & Parks, D.H. GTDB-Tk v2: memory friendly classification with the genome taxonomy database. *Bioinformatics* **38**, 5315–5316 (2022).
29. Jin, Y., Cai, F., Song, C., Liu, G. & Chen, C. Degradation of biodegradable plastics by anaerobic digestion: morphological, micro-structural changes and microbial community dynamics. *Sci. Total Environ.* **834**, 155167 (2022).
30. Jin, Y., Zhao, X., Lema, J.M., Liu, G. & Chen, C. Microplastic generation and persistence of biodegradable plastics under anaerobic conditions. *Environ. Sci. Technol.* **60**, 9565–9574 (2026).
31. Pessi, I.S., Eronen-Rasimus, E., Näkki, P., Thomas, D.N. & Kaartokallio, H. Bioplastic biodegradability shapes microbial communities in a coastal brackish environment. *ISME J.* **20**, wrag052 (2026).
32. Strotmann, U., et al. Testing the biodegradability of difficult compounds: a future challenge for the OECD/ISO standardization. *Appl. Microbiol. Biotechnol.* **110,** 112 (2026).
33. Meyer Cifuentes, I.E., et al. Comparative biodegradation analysis of three compostable polyesters by a marine microbial community. *Appl. Environ. Microbiol.* **89**, e01060–01023 (2023).
34. Lin, X., et al. A landfill serves as a critical source of microplastic pollution and harbors diverse plastic biodegradation microbial species and enzymes: study in large-scale landfills, China. *J. Hazard. Mater.* **457**, 131676 (2023).
35. International Organization for Standardization (ISO). *ISO 14853:2016 Plastics — Determination of the ultimate anaerobic biodegradation of plastic materials in an aqueous system — Method by measurement of biogas production* (ISO, Geneva, 2016).
36. American Public Health Association (APHA), American Water Works Association (AWWA), Water Environment Federation (WEF). *Standard Methods for the Examination of Water and Wastewater* (APHA, Washington D.C., 2005).
37. Dueholm, M.K.D., et al. MiDAS 5: global diversity of bacteria and archaea in anaerobic digesters. *Nat. Commun.* **15**, 5361 (2024).

Figures

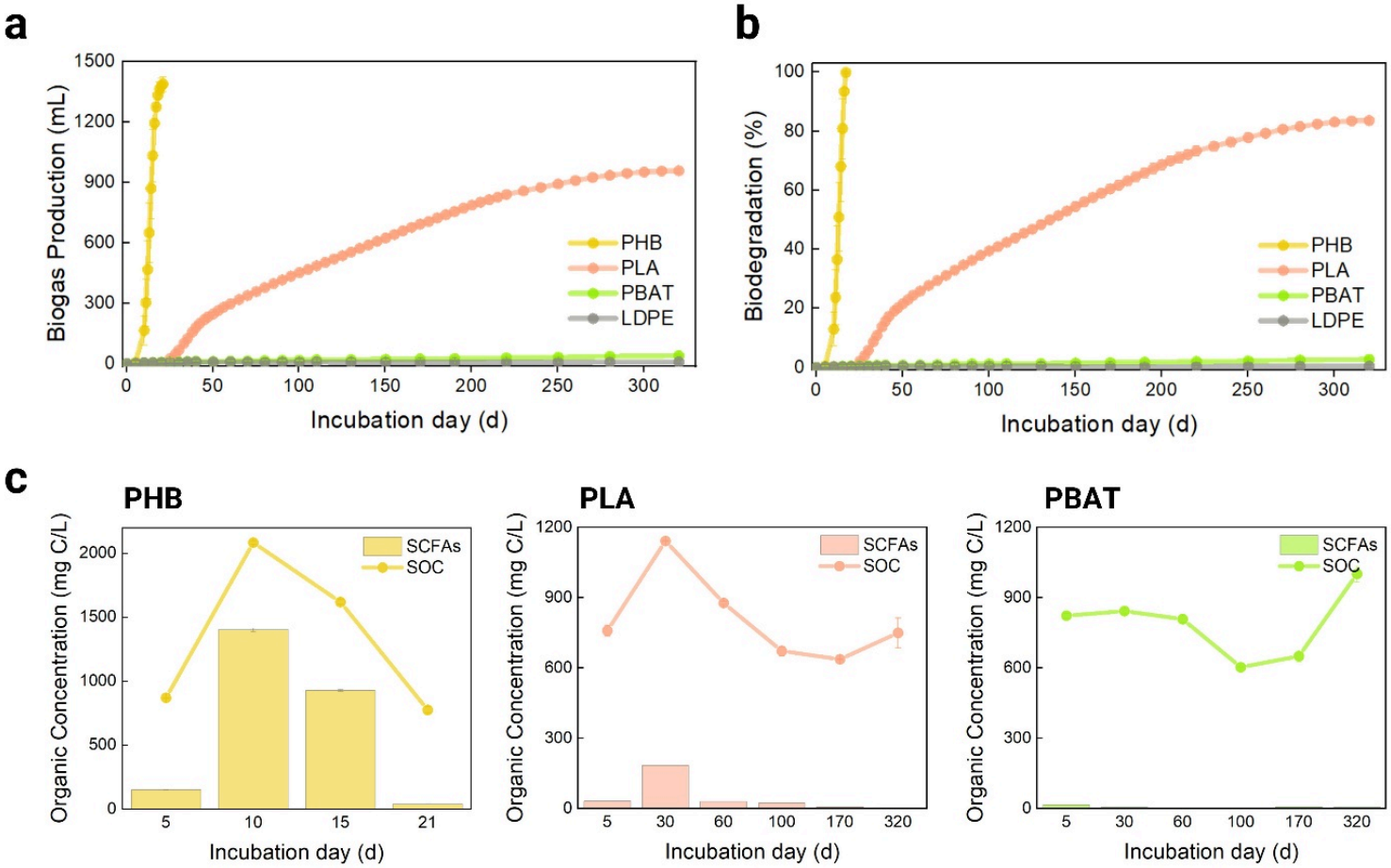

Figure 1

Divergent anaerobic degradation trajectories of BPs and LDPE (negative control) in landfill leachate over 320 d. a, Cumulative net biogas production calculated as the difference between biogas production from the plastic substrate-containing and blank assays. b, Biodegradation levels (mineralization) estimated from net biogas production, normalized to the theoretical maximum production calculated using the extended Buswell and Mueller equation. c, Short-chain fatty acids (SCFAs) and soluble organic carbon (SOC) profiles during biodegradation of PHB, PLA, and PBAT. Error bars represent standard deviation across replicates for each assay (n = 8–3, decreasing due to sacrificial sampling)

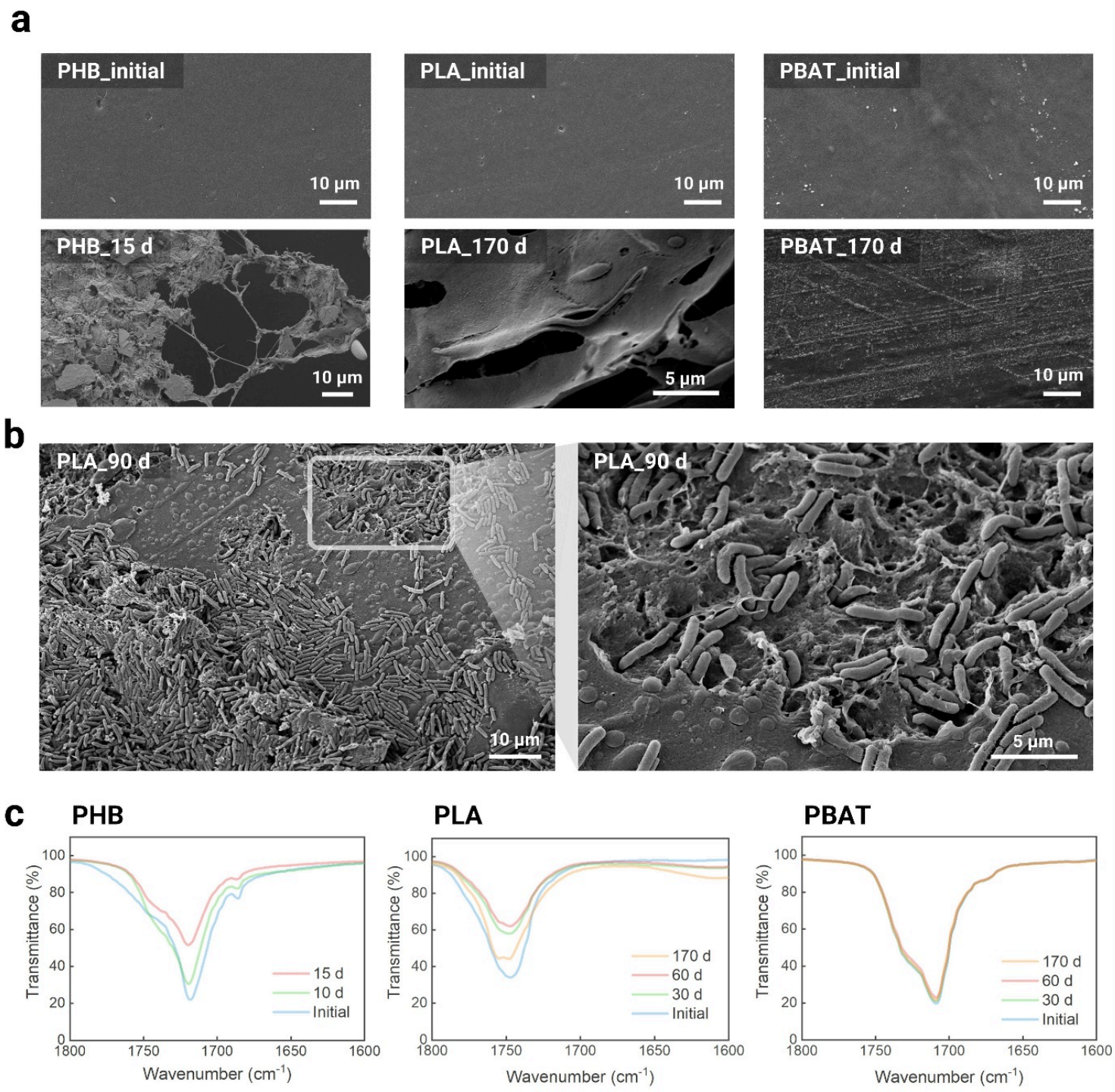

Figure 2

Structural and morphological changes of BPs during anaerobic biodegradation in landfill leachate. a, SEM micrographs of films before (initial) and during anaerobic incubation: PHB (15 d), PLA (170 d), and PBAT (170 d). b, Microbial colonization of PLA after 90 d of incubation in landfill leachate, showing dense surface-associated rod-shaped cells (left). The right panel shows a higher-magnification view of the dashed-boxed region. Scale bars are located at the bottom right of each image. c, FT-IR spectra of PHB, PLA, and PBAT showing time-dependent changes in the carbonyl (C=O) stretching region (1600–1800 cm^{-1}) with the progression of anaerobic degradation.

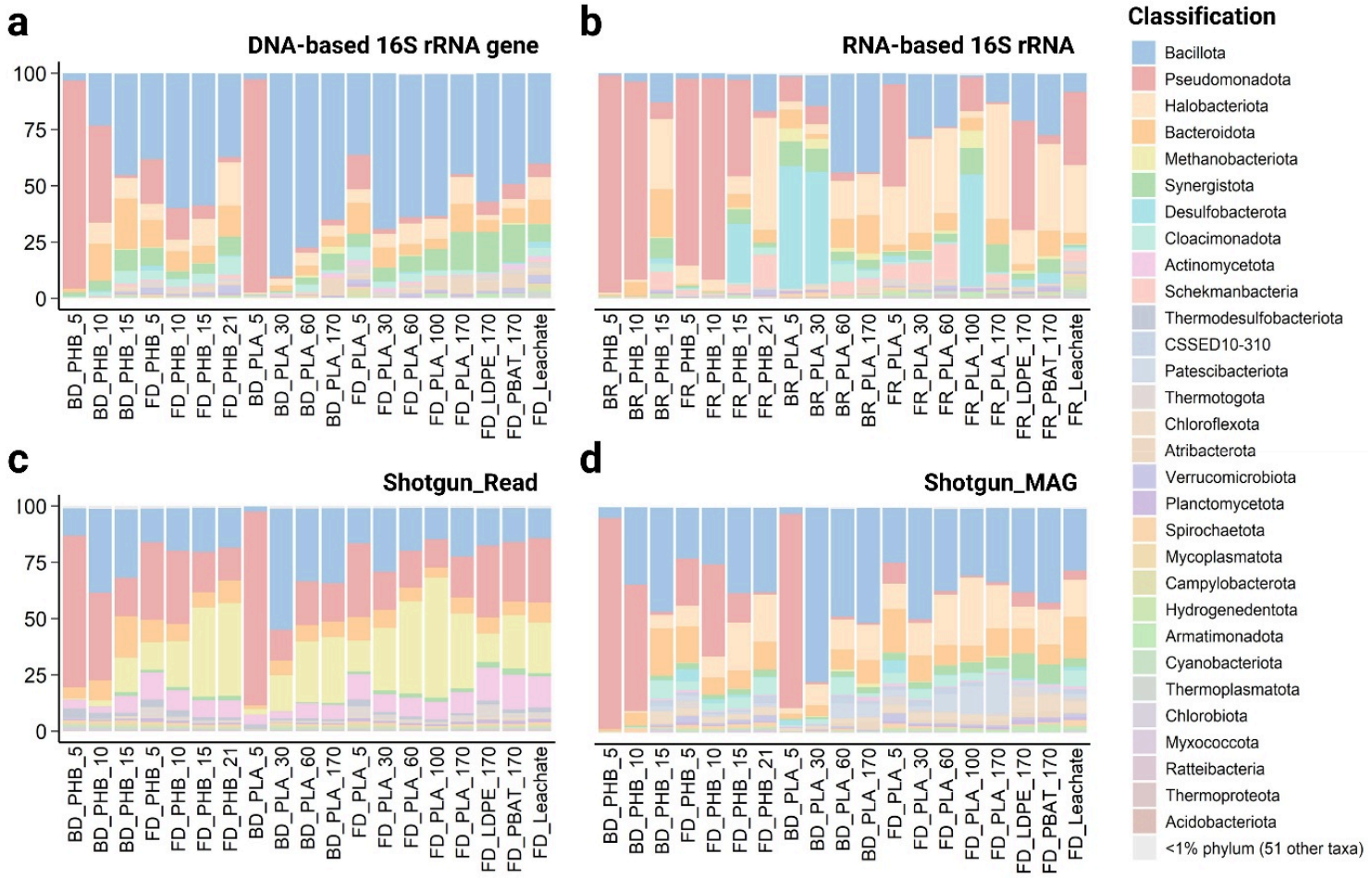

Figure 3

Microbial community composition across substrates, lifestyles, nucleic acid types, and sequencing approaches. Phylum-level taxonomic profiles from **a**, DNA-based 16S rRNA gene amplicon datasets classified with Greengenes2 [26]; **b**, RNA-based 16S rRNA amplicon datasets derived from cDNA and classified with Greengenes2; **c**, Shotgun metagenomes based on read-level classification with Kraken2 [27]; and **d**, Shotgun metagenomes based on MAG-based profiling using dereplicated MAGs classified with GTDB R226 [28]. Only phyla reaching >1% relative abundance in at least one sample are presented, and remaining low-abundance taxa are grouped as “51 other taxa”. Sample codes denote lifestyle (biofilm vs free-living), nucleic acid type (DNA vs RNA), substrate (PHB, PLA, PBAT, LDPE, and leachate inoculum), and incubation time (d) (See Table S3).

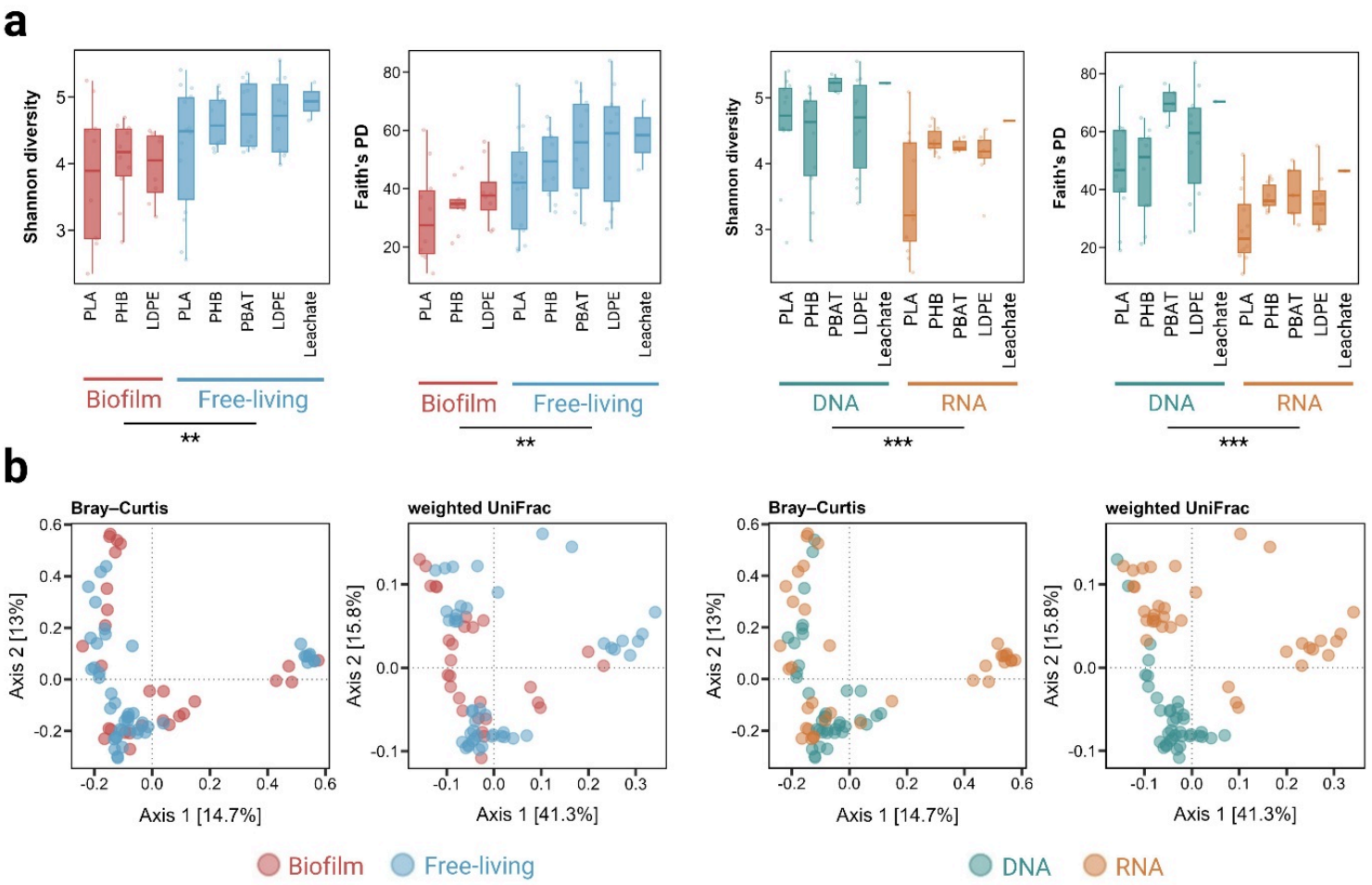

Figure 4

Microbial community diversity and dissimilarity across lifestyles and nucleic acid types. **a,** Alpha diversity of 16S rRNA (gene) amplicon datasets based on Shannon diversity and Faith's phylogenetic diversity. The left two panels compare biofilm and free-living communities using combined DNA- and RNA-derived datasets, whereas the right two panels compare DNA- and RNA-derived communities across all samples. **b,** Principal coordinates analysis (PCoA) of 16S rRNA (gene) amplicon-based community dissimilarities using Bray–Curtis and weighted UniFrac distances, colored by lifestyle (left) or nucleic acid type (right).

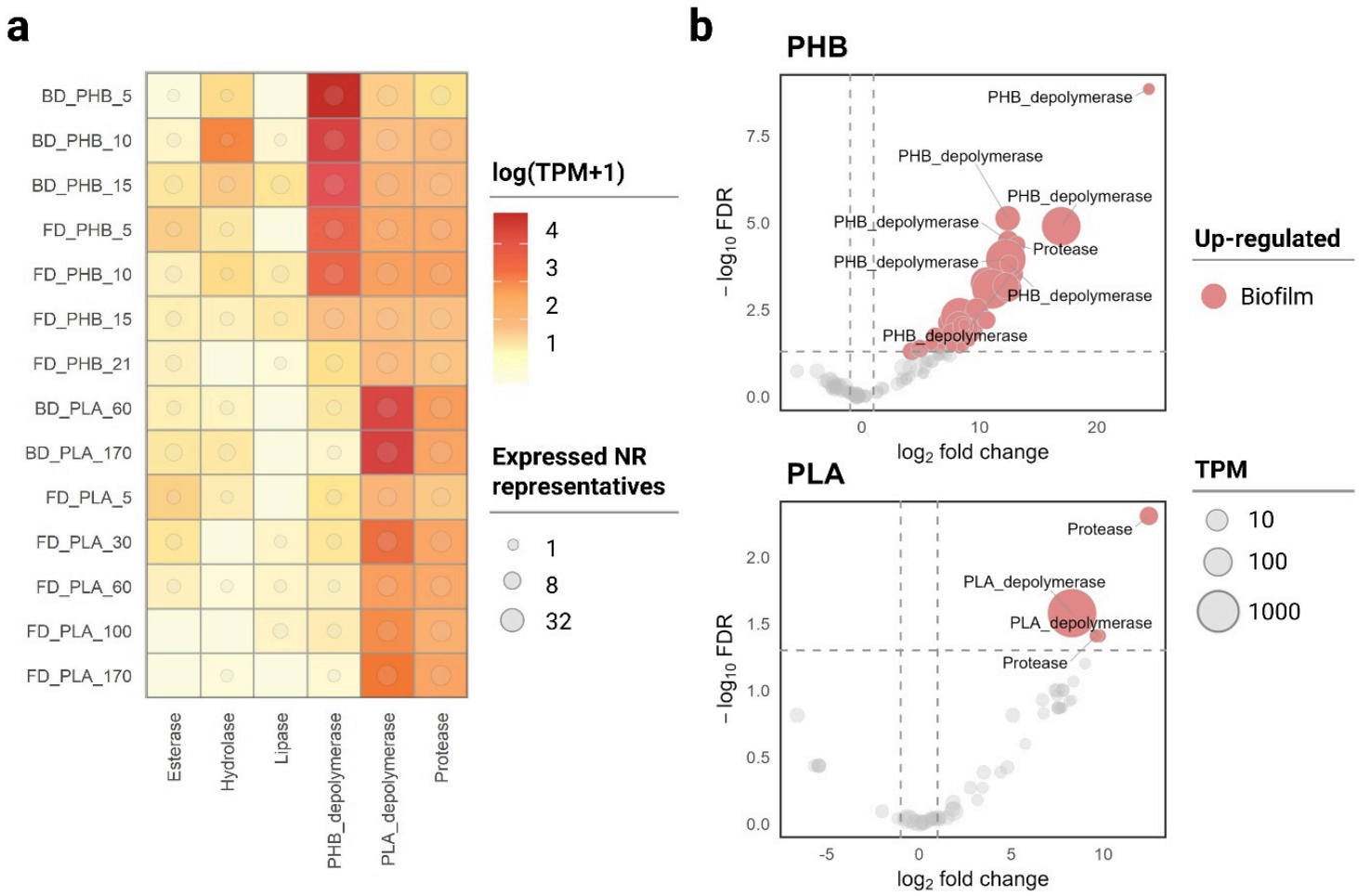

Figure 5

Transcript profiles and differential expression of enzyme families implicated in anaerobic biodegradation of PHB and PLA. **a**, Bubble heatmap of transcript abundance by enzyme families (color; $\log_{10}$[TPM + 1]) and the number of expressed NR representatives per family (circle size; NumReads > 0) across biofilm and free-living fractions incubated with PHB or PLA. **b**, Differential expression of NR representatives between biofilm and free-living fractions within PHB (top) and PLA (bottom) incubations. The *x*-axis shows $\log_2$ fold change (biofilm vs. free-living) and the y-axis shows $-\log_{10}$(FDR) from DESeq2 (Benjamini–Hochberg–adjusted Wald test) based on NumReads-derived count estimates. Point size indicates mean transcript abundance (TPM), and color denotes the fraction in which each representative is upregulated.



Figure 6

Genome-resolved narrowing from homolog-carrying MAGs to transcription-supported candidate MAGs and their time-resolved abundance patterns during PHB and PLA incubations. **a,** Maximum-likelihood phylogeny of genomes encoding depolymerase homologs, including transcription-supported MAGs recovered in this study (genome-level TPM ≥ 1; blue) and reference genomes represented in the curated PlasticDB–PAZy set (red). Branches are colored by phylum. Bubble overlays indicate genome-level

depolymerase transcript abundance (log_{10}[TPM+1]) for PHB (gold) and PLA (salmon). **b,** Bubble matrix summarizing sample-resolved MAG coverage and depolymerase transcription for representative candidate MAGs linked to PHB and PLA depolymerization. Rows denote MAGs grouped into PHB-associated and PLA-associated candidate sets. Bubble size represents log_{10}(coverage+1), where coverage is the per-sample genome-wide mean read depth. Bubble shading denotes depolymerase transcript abundance (log_{10}[TPM+1]), calculated from PHB- or PLA-associated depolymerase transcripts in the corresponding incubations.

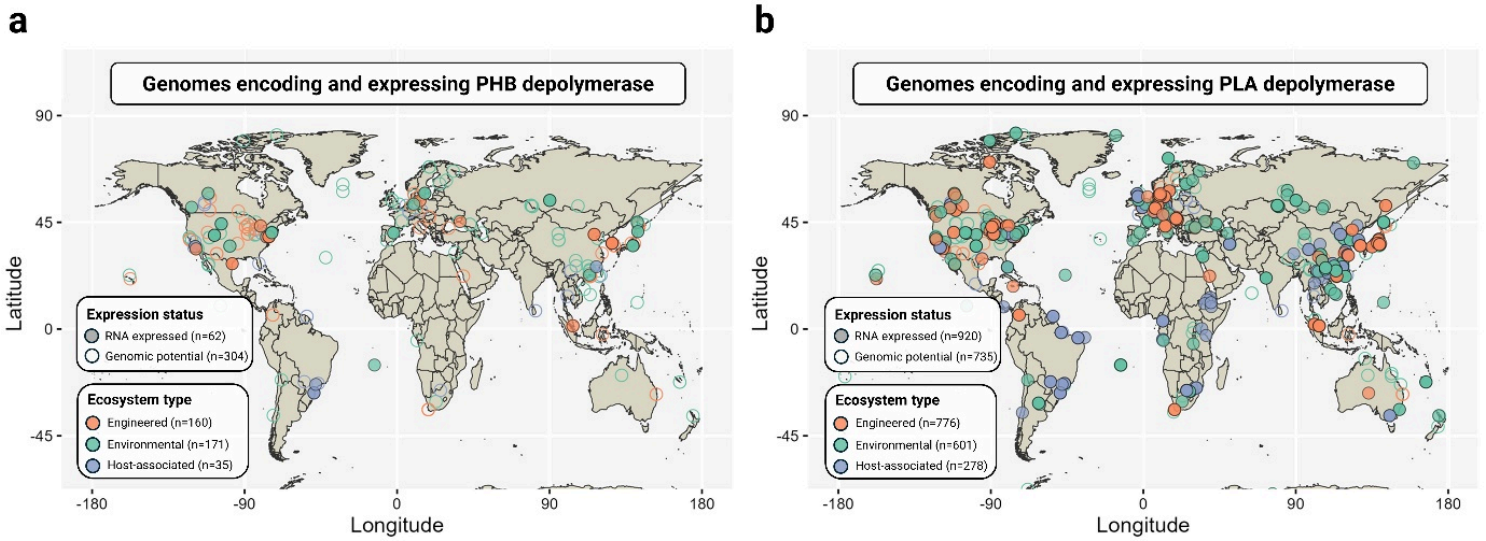

Figure 7

Ecological distribution of genomes encoding PHB- and PLA-depolymerase homologs. Georeferenced genomes encoding **a**, PHB-depolymerase homologs and **b**, PLA-depolymerase homologs. Genomes were compiled by first classifying the recovered MAGs from this study as potential or expressed on the basis of depolymerase homolog carriage and transcriptional support, and then expanding the corresponding lineages through targeted genome mining across public genome collections using GTDB-based taxonomic placement at the lowest resolved rank. All genomes were screened using the same annotation criteria throughout. Point color denotes inferred ecosystem category (engineered, environmental, or host-associated). Point outline denotes the MAG-derived status assigned to each lineage in the map. Expressed indicates lineages seeded by query MAGs with depolymerase transcriptional support in matched metatranscriptomes. Potential indicates lineages seeded by query MAGs classified only by depolymerase homolog carriage.

Supplementary Files

This is a list of supplementary files associated with this preprint. Click to download.

- Supplementarytablesrev17.xlsx
- SILandfillleachaterev21.docx